Supplement of The Cryosphere, 15, 2167–2186, 2021
https://doi.org/10.5194/tc-15-2167-2021-supplement

The Cryosphere Open Access EGU

Supplement of

Linking sea ice deformation to ice thickness redistribution using high-resolution satellite and airborne observations

Luisa von Albedyll et al.

Correspondence to: Luisa von Albedyll (luisa.von.albedyll@awi.de)

This supplement to the article **Linking sea ice deformation to ice thickness redistribution using high-resolution satellite and airborne observations** covers a description of the following aspects:

1. Calculation of deformation from sea ice drift (Sect. 1).
2. Estimate of the accumulated trajectory position error from a manual reference data set (Sect. 2).
3. Ice thickness profiles with level ice characterization for the Eastern and Central profile lines (Sect. 3).

1 Derivation of sea ice deformation from sea ice drift

This section provides further details about the calculation of deformation, described in the main article in Section 2.4. Deformation is quantified by strain rates that describe how an object distorts relative to a reference length-scale. The invariants of the 2D strain rate tensor are a normal component comprising tensile and compressive strain and termed divergence rate ($\dot{\epsilon}_{div}$) and a shear rate ($\dot{\epsilon}_{shear}$). Divergence and shear rate can be combined to yield the total deformation rate ($|\dot{\epsilon}|$). They are calculated from the spatial derivatives of the u, v components of the velocity grid ($\frac{\partial u}{\partial x}, \frac{\partial u}{\partial y}, \frac{\partial v}{\partial x}, \frac{\partial v}{\partial y}$):

$$\dot{\epsilon}_{div} = \frac{\partial u}{\partial x} + \frac{\partial v}{\partial y} \quad \text{(a)} \qquad \dot{\epsilon}_{shear} = \sqrt{\left(\frac{\partial u}{\partial x} - \frac{\partial v}{\partial y}\right)^2 + \left(\frac{\partial u}{\partial y} + \frac{\partial v}{\partial x}\right)^2} \quad \text{(b)} \qquad |\dot{\epsilon}| = \sqrt{\dot{\epsilon}_{div}^2 + \dot{\epsilon}_{shear}^2} \quad \text{(c)} \tag{1}$$

To calculate the spatial derivatives of the ice drift velocity fields, we used a linear approximation based on Green's Theorem that relates the double integral over a plane to the line integral along a simple curve surrounding the plane. We discretized the curve applying the trapezoid method that linearly interpolates velocity between the vertices (i) of the grid cells (e.g. Kwok et al., 2008; Dierking et al., 2020). The spatial derivatives are thus given by:

$$\frac{\partial u}{\partial x} = \frac{1}{A}\oint_C u\,dy = \frac{1}{2A}\sum_{i=1}^{N}(u_{i+1}+u_i)(y_{i+1}-y_i) \qquad \frac{\partial v}{\partial x} = \frac{1}{A}\oint_C v\,dy = \frac{1}{2A}\sum_{i=1}^{N}(v_{i+1}+v_i)(y_{i+1}-y_i)$$
$$\frac{\partial u}{\partial y} = -\frac{1}{A}\oint_C u\,dx = -\frac{1}{2A}\sum_{i=1}^{N}(u_{i+1}+u_i)(x_{i+1}-x_i) \qquad \frac{\partial v}{\partial y} = -\frac{1}{A}\oint_C v\,dx = -\frac{1}{2A}\sum_{i=1}^{N}(v_{i+1}+v_i)(x_{i+1}-x_i) \tag{2}$$

where A is the area surrounded by the line integral. We calculated the spatial derivatives from the spatially filtered velocity fields with a spatial resolution of 700x700 m. We considered for every derivative a set of four grid cells. Hence, we used eight vertices ($N = 8$) to describe the line integral around the plane. For a gridded field, we can simplify this approach. For example, the 8pt ring-integral for a subset of the u-component in x-direction is:

$$\begin{aligned}\frac{\partial u}{\partial x} =& \frac{1}{2A}[(u_2+u_1)(y_2-y_1)+(u_3+u_2)(y_3-y_2)+(u_4+u_3)(y_4-y_3)+\\ &(u_5+u_4)(y_5-y_4)+(u_6+u_5)(y_6-y_5)+(u_7+u_6)(y_7-y_6)+(u_8+u_7)(y_8-y_7)+(u_8+u_1)(y_8-y_1)]\end{aligned} \tag{3}$$

Thanks to the regular grid, we can simplify:

$$\begin{aligned} 0 &= (y_4-y_3) = (y_5-y_4) = (y_8-y_7) = (y_1-y_8)\\ \Delta y &= -(y_2-y_1) = -(y_3-y_2) = (y_6-y_5) = (y_7-y_6)\\ \Delta x &= \Delta y\\ A &= (2\Delta y)\times(2\Delta x) = 4\Delta y\Delta y \end{aligned} \tag{4}$$

with Δy =700 m.
Then, the derivate is:

$$\begin{aligned}\frac{\partial u}{\partial x} &= \frac{1}{8\Delta y \Delta y}\Delta y[2u_6 + u_5 + u_7) - (2u_2 + u_1 + u_3)] \\ &= \frac{(2u_6 + u_5 + u_7) - (2u_2 + u_1 + u_3)}{8\Delta y}\end{aligned} \tag{5}$$

This is equivalent to calculating the convolution of the u-component with a 3x3 Sobel kernel and normalizing it by a factor of 8 Δy. For example, $\frac{\partial u}{\partial x}$ is calculated:

$$\frac{\partial u}{\partial x} = \frac{1}{8\Delta y}\, k_x * u = \frac{1}{8\Delta y}\begin{pmatrix} -1 & 0 & 1 \\ -2 & 0 & 2 \\ -1 & 0 & 1 \end{pmatrix} * u \tag{6}$$

We located the result to the center of the four grid cells. Moving with a step width of one grid cell, the grid spacing of the deformation fields remained 700 m.

2 Estimate of the accumulated trajectory position error from a manual reference data set

This section provides further details about the uncertainty estimates of the Lagrangian tracking described in Section 2.5.1. We quantified the **accumulated trajectory position error** from manual tracking of multi-year ice floes located in the refrozen polynya (see Fig. 1a). Fig. S1 shows how the **accumulated trajectory position error** increased from maximum 210 m (after the second time step) to 2150 m (last time step). On average, the error increased from 51 m to 1050 m (red dots, Fig. S1). We estimated the uncertainty for each time step as a linear function that passed through the smallest grid size, i.e., 700 m and 2150 m at time step 0 and 29, respectively (dashed line in Fig. S1).

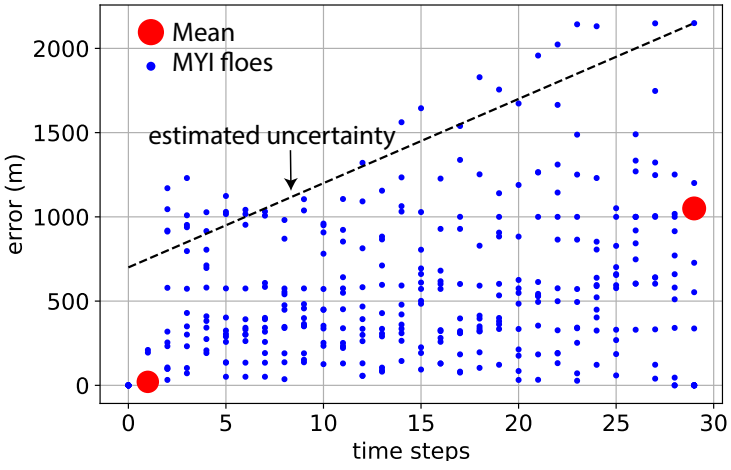

Figure S1. Difference between manual reference track and calculated trajectory for each time step. The mean of the differences after the second and the last time step are shown in red. The dashed black line gives the estimated uncertainty for each time step.

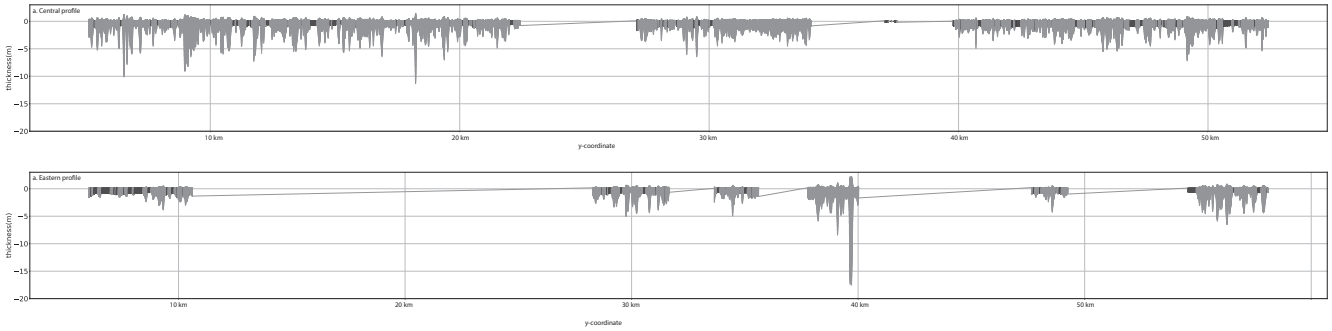

Figure S2. Ice thickness profile of the a. Central and b. Eastern profile. The black and gray colors distinguish between level and deformed ice, respectively. Note the different degrees of deformation, depicted by the areal fraction of level ice and the total thickness of the ridges.

3 Ice thickness profiles with level ice characterization for Eastern and Central profile line

This section provides further details about the ice thickness profiles and the level ice classification. For details on the method, the geographic location, and the classification of the Northern profile line, please see Section 2.1, Figure 1, and Figure 6 in the main article, respectively. We classified level ice and deformed ice following the level ice classification of Rabenstein et al. (2010). For details on the calculation, please see Section 2.1 of the main article. The Northern profile is displayed in Fig. 6.

References

Dierking, W., Stern, H. L., and Hutchings, J. K.: Estimating statistical errors in retrievals of ice velocity and deformation parameters from satellite images and buoy arrays, The Cryosphere, 14, 2999–3016, https://doi.org/10.5194/tc-14-2999-2020, 2020.

Kwok, R., Hunke, E. C., Maslowski, W., Menemenlis, D., and Zhang, J.: Variability of sea ice simulations assessed with RGPS kinematics, Journal of Geophysical Research, 113, https://doi.org/10.1029/2008jc004783, 2008.

Rabenstein, L., Hendricks, S., Martin, T., Pfaffhuber, A., and Haas, C.: Thickness and surface-properties of different sea-ice regimes within the Arctic Trans Polar Drift: Data from summers 2001, 2004 and 2007, Journal of Geophysical Research, 115, https://doi.org/10.1029/2009jc005846, 2010.